

# Experimental and Theoretical Investigation into the Correlation between Mass and Ion Mobility for Choline and Other Ammonium Cations in N<sub>2</sub>

Hyungjun Kim,<sup>†</sup> Hugh I. Kim,<sup>\*,§</sup> Paul V. Johnson,<sup>‡</sup> Luther W. Beegle,<sup>\*,‡</sup> J. L. Beauchamp,<sup>§</sup> William A. Goddard,<sup>†</sup> and Isik Kanik<sup>‡</sup>

Materials and Process Simulation Center, Beckman Institute, California Institute of Technology, Pasadena, California 91125, Noyes Laboratory of Chemical Physics, California Institute of Technology, Pasadena, California 91125, and Jet Propulsion Laboratory, California Institute of Technology, Pasadena, California 91109

A number of tertiary amine and quaternary ammonium cations spanning a mass range of 60–146 amu (trimethylamine, tetramethylammonium, trimethylethylammonium, *N,N*-dimethylaminoethanol, choline, *N,N*-dimethylglycine, betaine, acetylcholine, (3-carboxypropyl)trimethylammonium) were investigated using electrospray ionization ion mobility spectrometry. Measured ion mobilities demonstrate a high correlation between mass and mobility in N<sub>2</sub>. In addition, identical mobilities within experimental uncertainties are observed for structurally dissimilar ions with similar ion masses. For example, dimethylethylammonium (88 amu) cations and protonated *N,N*-dimethylaminoethanol cations (90 amu) show identical mobilities (1.93 cm<sup>2</sup> V<sup>-1</sup> s<sup>-1</sup>) though *N,N*-dimethylaminoethanol contains a hydroxyl functional group while dimethylethylammonium only contains alkyl groups. Computational analysis was performed using the modified trajectory (TJ) method with nonspherical N<sub>2</sub> molecules as the drift gas. The sensitivity of the ammonium cation collision cross sections to the details of the ion–neutral interactions was investigated and compared to other classes of organic molecules (carboxylic acids and abiotic amino acids). The specific charge distribution of the molecular ions in the investigated mass range has an insignificant affect on the collision cross section.

The development of soft ionization methods such as electrospray ionization (ESI)<sup>1</sup> have expanded the application of ion mobility spectrometry (IMS)<sup>2,3</sup> to structural investigations of nonvolatile biomolecules in the gas phase.<sup>4</sup> ESI allows soft sampling by transferring intact ions directly from the solution

phase to the gas phase. Using this distinctive advantage of ESI, the shapes and sizes of various biomolecular ions from monomeric molecules to macrosized protein complexes have been investigated. The combination of ESI and IMS has facilitated conformational studies of macroions including clusters (oligomers),<sup>5–7</sup> peptides,<sup>8,9</sup> and proteins.<sup>10–12</sup> In addition, ion mobilities of organic molecules such as amino acids,<sup>13,14</sup> carboxylic acids,<sup>15</sup> and dinucleotides,<sup>16</sup> as well as other organic molecules,<sup>17,18</sup> have been reported.

To provide a firm foundation for studies of the shapes of complex organic molecular ions using IMS, many research groups have endeavored to develop theoretical models to predict ion mobilities and related cross sections of gas-phase molecular ions. Griffin et al.<sup>19</sup> have shown that mass and mobility are only correlated on the order of 20% within a collection of structurally unrelated compounds spanning a mass range of ~70–500 amu. The correlations are improved up to 2% when only structurally related compounds are considered. Karpas and co-workers have established models to predict the mobility for a number of compound classifications including acetyls, aromatic amines, and aliphatic amines drifting in He, N<sub>2</sub>, air, Ar, CO<sub>2</sub>, and SF<sub>6</sub>.<sup>20,21</sup> Our

\* To whom correspondence should be addressed. E-mail: Luther.Beegle@jpl.nasa.gov.

<sup>†</sup> Materials and Process Simulation Center, Beckman Institute.

<sup>‡</sup> Jet Propulsion Laboratory.

<sup>§</sup> Noyes Laboratory of Chemical Physics.

(1) Fenn, J. B.; Mann, M.; Meng, C. K.; Wong, S. F.; Whitehouse, C. M. *Science* **1989**, *246*, 64–71.

(2) Shumate, C. B.; Hill, H. H. *Anal. Chem.* **1989**, *61*, 601–606.

(3) Wittmer, D.; Luckenbill, B. K.; Hill, H. H.; Chen, Y. H. *Anal. Chem.* **1994**, *66*, 2348–2355.

(4) Creaser, C. S.; Griffiths, J. R.; Bramwell, C. J.; Noreen, S.; Hill, C. A.; Thomas, C. L. P. *Analyst* **2004**, *129*, 984–994.

(5) Gidden, J.; Ferzoco, A.; Baker, E. S.; Bowers, M. T. *J. Am. Chem. Soc.* **2004**, *126*, 15132–15140.

(6) Julian, R. R.; Hodyss, R.; Kinnear, B.; Jarrold, M. F.; Beauchamp, J. L. *J. Phys. Chem. B* **2002**, *106*, 1219–1228.

(7) Counterman, A. E.; Clemmer, D. E. *J. Phys. Chem. B* **2001**, *105*, 8092–8096.

(8) Kaleta, D. T.; Jarrold, M. F. *J. Phys. Chem. A* **2002**, *106*, 9655–9664.

(9) Wu, C.; Siems, W. F.; Klasmeier, J.; Hill, H. H. *Anal. Chem.* **2000**, *72*, 391–395.

(10) Shelimov, K. B.; Clemmer, D. E.; Hudgins, R. R.; Jarrold, M. F. *J. Am. Chem. Soc.* **1997**, *119*, 2240–2248.

(11) Hudgins, R. R.; Woenckhaus, J.; Jarrold, M. F. *Int. J. Mass Spectrom.* **1997**, *165*, 497–507.

(12) Clemmer, D. E.; Jarrold, M. F. *J. Mass Spectrom.* **1997**, *32*, 577–592.

(13) Beegle, L. W.; Kanik, I.; Matz, L.; Hill, H. H. *Anal. Chem.* **2001**, *73*, 3028–3034.

(14) Johnson, P. V.; Kim, H. I.; Beegle, L. W.; Kanik, I. *J. Phys. Chem. A* **2004**, *108*, 5785–5792.

(15) Kim, H. I.; Johnson, P. V.; Beegle, L. W.; Beauchamp, J. L.; Kanik, I. *J. Phys. Chem. A* **2005**, *109*, 7888–7895.

(16) Gidden, J.; Bowers, M. T. *Eur. Phys. J. D* **2002**, *20*, 409–419.

(17) Asbury, G. R.; Klasmeier, J.; Hill, H. H. *Talanta* **2000**, *50*, 1291–1298.

(18) Asbury, G. R.; Wu, C.; Siems, W. F.; Hill, H. H. *Anal. Chim. Acta* **2000**, *404*, 273–283.

(19) Griffin, G. W.; Dzidic, I.; Carroll, D. I.; Stillwel, R. N.; Horning, E. C. *Anal. Chem.* **1973**, *45*, 1204–1209.

(20) Berant, Z.; Karpas, Z. *J. Am. Chem. Soc.* **1989**, *111*, 3819–3824.

(21) Karpas, Z.; Berant, Z. *J. Phys. Chem.* **1989**, *93*, 3021–3025.

laboratory has applied a 12–4 potential model in studies of amino acids and carboxylic acids drifting in N<sub>2</sub> and CO<sub>2</sub>.<sup>14,15</sup> Recently, Steiner et al. have reported predictions of mobilities for a series of different classes of amines (primary, secondary, tertiary) in various drift gases, such as He, Ne, Ar, N<sub>2</sub>, and CO<sub>2</sub>, using several theoretical models (rigid-sphere, polarization-limit, 12-6-4, and 12–4 potential model).<sup>22</sup>

Computational modeling related to interpretation of IMS data has been developed by several groups. Efforts toward theoretical ion mobility predictions using computational methods face difficulties associated with complicated collision integrals and the design of functions to accurately describe the ion–neutral interaction potential. Bowers and co-workers have proposed a project approximation method, which is based on a hard-sphere description of the interaction potential.<sup>23</sup> The trajectory (TJ) method, which has been proposed by Jarrold and co-workers, adopts more realistic soft-core interactions.<sup>24</sup>

Ion mobility constants ( $K$ ) can be derived from the collision cross section using the equation<sup>25</sup>

$$K = \frac{(18\pi)^{1/2}}{16} \frac{1}{\mu^{1/2}} \frac{ze}{(k_B T)^{1/2} \Omega_D} \frac{1}{N} \quad (1)$$

where  $\mu$  is reduced mass,  $N$  is the number density of the neutral gas molecule, and  $z$  is the charge of the ion. The collision cross section,  $\Omega_D$ , is given by<sup>24</sup>

$$\Omega_D = \frac{1}{8\pi^2} \int_0^{2\pi} d\theta \int_0^\pi d\phi \int_0^{2\pi} d\gamma \frac{\pi \left(\frac{\mu}{8k_B T}\right)^3}{g} \int_0^\infty dg e^{-\mu/2k_B T g^5} \int_0^\infty db 2b(1 - \cos \chi(\theta, \phi, \gamma, g, b)) \quad (2)$$

and  $\theta$ ,  $\phi$ , and  $\gamma$  are the three-dimensional collision angles,  $g$  is the relative velocity, and  $b$  is the impact parameter. Because the scattering angle  $\chi(\theta, \phi, \gamma, g, b)$  depends on the pairwise potential between the ion and neutral gas molecules, the accuracy of computed cross section values is determined by the quality of the interaction potential model. The potential employed in the TJ method<sup>24</sup> for a He drift gas is given by

$$\Phi(\theta, \phi, \gamma, b, r) = 4\epsilon \sum_i^n \left[ \left( \frac{\sigma}{r_i} \right)^{12} - \left( \frac{\sigma}{r_i} \right)^6 \right] - \frac{\alpha \left( \frac{ze}{n} \right)^2}{2} \left[ \left( \sum_i^n \frac{x_i}{r_i^3} \right)^2 + \left( \sum_i^n \frac{y_i}{r_i^3} \right)^2 + \left( \sum_i^n \frac{z_i}{r_i^3} \right)^2 \right] \quad (3)$$

The first term is a sum over short-range van der Waals interactions, and the second term represents long-range ion-induced dipole interactions. In the expression,  $\epsilon$  is the depth of the potential well,  $\sigma$  is the value of distance ( $r$ ) between the centers of mass of

the each atom in the ion and neutral gas molecule at the potential minimum, and  $\alpha$  is the neutral polarizability. The coordinates,  $r_i$ ,  $x_i$ ,  $y_i$ , and  $z_i$ , are defined by the relative positions of the atoms with respect to the neutral. Utilizing the given ion–neutral interaction potential functions, the integrals in eq 2 can be processed numerically. Monte Carlo integration schemes are used for the integration over  $\theta$ ,  $\phi$ ,  $g$ , and  $b$ . The numerical integration over  $g$  is performed using a combination of the Runge–Kutta–Gill integration method and the Adams–Moulton predictor–corrector integration method.

Choline is a precursor for phosphatidylcholine, sphingomyelin, and other important biological molecules.<sup>26</sup> Further, it is a component of cell membrane lipids in biological systems, and it plays an important role in their repair. Choline can be oxidized to betaine, which is readily demethylated to yield *N,N*-dimethylglycine.<sup>26</sup> Decomposition of choline yields trimethylamine and dimethylamine.<sup>27</sup> Searching for lipids and their components (i.e., choline) may be a valuable strategy in the search for evidence of extinct or extant life elsewhere in the cosmos. Under the high oxidizing conditions and significant ultraviolet flux found on the surface of Mars, one would expect decomposition products of lipids to include various alkylamines.<sup>28</sup>

In the present study, mobilities have been measured for a number of quaternary and tertiary ammonium cations related to choline and its derivatives drifting in N<sub>2</sub>. Of particular interest was the possible dependence of mass–mobility correlations with the heavy atom (C, N, O) complements present in the molecular ion, comparing, for example, alkylated ammonium ions to abiotic amino acids (betaine and *N,N*-dimethylglycine). A modified TJ method for the ion–neutral interaction, to account for the potential associated with the nonspherical drift gas N<sub>2</sub>, has been applied to predict cross sections of these polyatomic ammonium cations and to test the sensitivity of collision cross section to details of the ion–neutral interaction. Comparisons of the results from the ammonium cations to other classes of organic molecules (carboxylic acids and abiotic amino acids) are presented. The origin of the observed correlation between mass and mobility of ammonium cations is discussed.

## EXPERIMENTAL SECTION

**Chemicals and Reagents.** All the compounds studied in this work were purchased from Sigma Aldrich (St. Louis, MO) and were used without further purification. All solvents (water, methanol, acetic acid) were HPLC grade and were purchased from EMD Chemicals Inc. (Gibbstown, NJ). Quaternary ammonium samples were prepared by dissolving known quantities of ammonium ions in a solvent consisting of 50% water and 50% methanol by volume to give sample concentrations in the range of 100  $\mu$ M. Tertiary amine samples were prepared as 300  $\mu$ M in a solvent of 50:50 water and methanol with 1% acetic acid by volume.

**Electrospray Ionization Ion Mobility Spectrometer.** The ESI-IMS instrument and the data acquisition system used in this investigation were based on designs previously described by Hill and co-workers<sup>17,29</sup> and have been described in detail by Johnson

(22) Steiner, W. E.; English, W. A.; Hill, H. H. *J. Phys. Chem. A* **2006**, *110*, 1836–1844.

(23) Vonhelden, G.; Hsu, M. T.; Kemper, P. R.; Bowers, M. T. *J. Chem. Phys.* **1991**, *95*, 3835–3837.

(24) Mesle, M. F.; Hunter, J. M.; Shvartsburg, A. A.; Schatz, G. C.; Jarrold, M. F. *J. Phys. Chem.* **1996**, *100*, 16082–16086.

(25) Mason, E. A.; O'hara, H.; Smith, F. J. *J. Phys. B* **1972**, *5*, 169–176.

(26) Blusztajn, J. K. *Science* **1998**, *281*, 794–795.

(27) Zeisel, S. H.; Dacosta, K. A.; Youssef, M.; Hensey, S. J. *Nutr.* **1989**, *119*, 800–804.

(28) McHowat, J.; Jones, J. H.; Creer, M. H. *J. Lipid Res.* **1996**, *37*, 2450–2460.

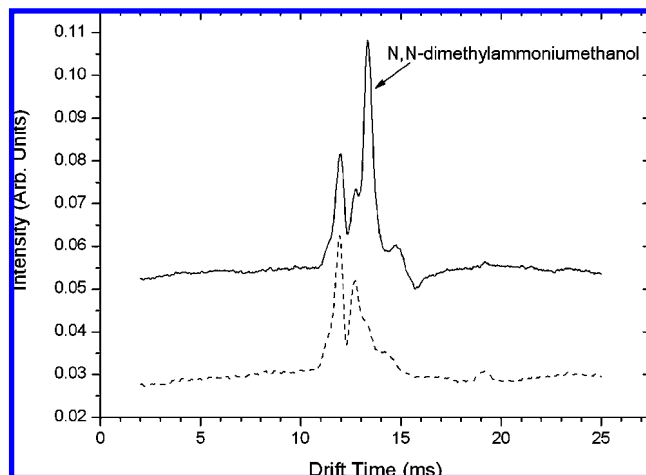


**Figure 1.** Examples of the ion mobility spectra taken in this study. Shown are two spectra taken in 730 Torr  $N_2$ . The electric field strength and the temperature of the drift tube were 292 V/cm and 473 K, respectively. The dash curve is a spectrum taken with pure solvent being introduced to the electrospray needle while the solid curve is a spectrum of solvent and 300  $\mu$ M  $N,N$ -dimethylammoniummethanol. The two spectra were smoothed (10 point adjacent averaging) and shifted in intensity by an additive constant to avoid overlap. The  $N,N$ -dimethylammoniummethanol feature is indicated in the figure. The unlabeled features correspond to ionized solvent (water, methanol, acetic acid) and atmospheric constituents ionized through proton transfer (due to the open nature of the ESI-IMS instrument).

et al.<sup>14</sup> The drift length of the ion mobility spectrometer was 13.65 cm and was operated in the positive mode. A drift voltage of 3988 V, corresponding to electric field strength of 292 V/cm, was employed. All measurements were made at local atmospheric pressure ( $\sim$ 730 Torr) while a counterflow of the preheated drift gas was introduced at the detection end of the drift region at a flow rate of  $\sim$ 800 mL/min. The sample solution was delivered by an Eldex Micropro liquid chromatography pump at a flow rate of 3  $\mu$ L/min into a stainless steel electrospray needle, which was held at a potential 3–4 kV above the entrance to the desolvation region of the spectrometer. The gap between the electrospray needle and the entrance electrode was  $\sim$ 2 cm.

Ions were introduced into the drift region through the ion gate in 0.2-ms pulses. Signals collected at the Faraday cup were amplified by a factor of  $10^9$  (Stanford Research Systems model SR570 low-noise current preamplifier) and recorded as a function of drift time in 0.02-ms-wide channels. Typically, 1000 individual 0–25-ms scans were averaged to produce the final spectra used in the analysis. Resolution of the instrument was found to be  $\sim$ 0.43 ms full width at half-maximum (FWHM) with drift times in the range 12–17 ms for the ions studied and the parameters employed in these experiments.

Throughout this work, it was assumed that ESI of the prepared samples resulted in singly charged ammonium cations. The assumption was confirmed by ESI mass spectrometric analysis using a Finnigan LCQ Deca XP ion trap mass spectrometer. The mass spectra of all nine samples in the present study show singly charged monomeric molecular cations as the major ionic species. Since the experiments were conducted with the drift cell at 473 K, it was further assumed that there was no significant water cluster formation based on previous IMS–MS studies.<sup>18,30</sup>

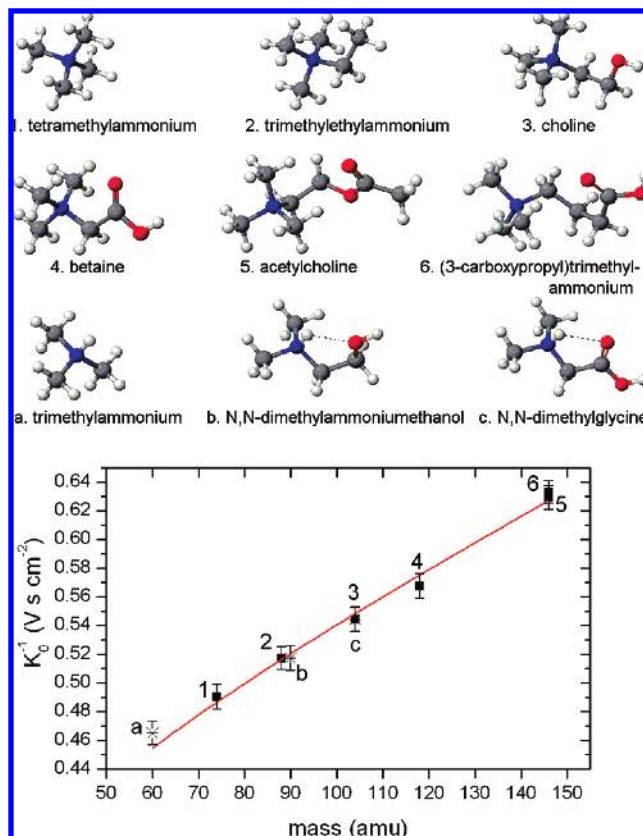


**Figure 2.** Plot of  $K_0^{-1}$  for 3° and 4° ammonium cations drifting in  $N_2$  versus ion mass. Experimentally determined data for 3° ammonium and 4° ammonium cations are shown as asterisks and solid squares, respectively. The solid line is the fit of the 12–4 potential model to the ammonium cation data set. DFT optimized structure of each numerically or alphabetically labeled ion is shown above. Optimized geometries are obtained at B3LYP/6-31G\*\* level. The hydrogen bonds are indicated with dashed lines.

Reduced ion mobilities,  $K_0$ , were determined from the recorded spectra and the experimental parameters according to the usual relation,

$$K_0 = \left( \frac{273K}{T} \right) \left( \frac{P}{760 \text{ Torr}} \right) \frac{D^2}{Vt} \quad (4)$$

where  $V$  is the voltage drop across the drift region,  $D$  is the drift length,  $t$  is the drift time,  $P$  is the pressure, and  $T$  is the temperature. With the above parameters expressed in units of V, cm, s, Torr, and K, respectively, eq 4 gave the reduced mobility in the typical units of  $\text{cm}^2 \text{V}^{-1} \text{s}^{-1}$ . The experimental uncertainties of the determined  $K_0$  values are estimated to be  $\sim$ 3% based on the half width at half-maximum (HWHM) of each drift time peak in the averaged ion mobility spectra.

**Computational Modeling.** More than 500 possible molecular conformations were investigated through dihedral angles of  $-180^\circ$  to  $180^\circ$  at the PM5 level using CAChe 6.1.12 (Fujitsu, Beaverton, OR). Then, the lowest-energy structures were determined using density functional theory (DFT) with a number of

(29) Wu, C.; Siems, W. F.; Asbury, G. R.; Hill, H. H. *Anal. Chem.* **1998**, *70*, 4929–4938.

(30) Asbury, G. R.; Hill, H. H. *Anal. Chem.* **2000**, *72*, 580–584.



candidate low-energy structures from the previous PM5 calculations. DFT calculations were performed using Jaguar 6.0 (Schrödinger, Inc., Portland, OR) utilizing the Becke three-parameter functional (B3)<sup>31</sup> combined with the correlation functional of Lee, Yang, and Parr (LYP),<sup>32</sup> using the 6-31G\*\* basis set.<sup>33</sup> The optimized structures of ammonium cations investigated in the present study are shown in Figure 2.

The TJ method,<sup>24</sup> originally developed by Jarrold and co-workers, was modified to describe the interaction between ions and an N<sub>2</sub> drift gas and expand the applicability of the TJ method beyond cases of ions drifting in He. As shown in eq 3, the potential used in the original TJ method consists of two terms representing van der Waals and ion-induced dipole interactions, which are characterized by the Lennard-Jones parameters ( $\epsilon$ ,  $\sigma$ ) and the neutral polarizability ( $\alpha$ ), respectively. We set the polarizability of N<sub>2</sub> at the experimentally determined value<sup>34</sup> of  $1.710 \times 10^{-24}$  cm<sup>3</sup> and took the Lennard-Jones parameters described in the universal force field,<sup>35</sup> which is a general purpose force field optimized for all the elements in the periodic table. Due to the linear geometry of N<sub>2</sub>, two more consequences should be additionally taken into account; the ion-quadrupole interaction and the orientation of the molecule. We mimic the quadrupole moment of N<sub>2</sub>,  $(-4.65 \pm 0.08) \times 10^{-40}$  C cm<sup>2</sup>,<sup>36</sup> by displacing charges by negative  $q$  ( $0.4825e$ ) to each nitrogen atom and one positive  $2q$  at the center of the nitrogen molecule. Hence, the ion-quadrupole potential can be expressed with simple summations of partial charges as follows:

$$\Phi_{IQ} = \sum_{j=1}^3 \sum_i^n \frac{z_i z_j e^2}{r_{ij}} \quad (5)$$

where indexes  $i$  and  $j$  denote the atoms of the ion, three points of N<sub>2</sub>,  $j = 1$  and  $3$  indicate the two nitrogen atoms, and  $j = 2$  indicates the center of mass position of N<sub>2</sub>.

To consider the orientation of the nitrogen molecule rigorously, all possible trajectories with varying molecular orientations were taken into account. It has been widely accepted that the ion field does not exclusively quench the rotational angular momentum of the neutral molecule and only partial locking occurs during the collision process.<sup>37,38</sup> Thus, we assumed that the interaction potential averaged over the rotational degree of freedom generates an appropriated average impact parameter.<sup>39</sup> The calculated rotation time of a N<sub>2</sub> molecule ( $\sim 620$  ns) implies that approximately three molecular rotations occur during a collision between an ion and N<sub>2</sub> taking place ( $\sim 2$  ps). The orientations of N<sub>2</sub> are sampled along with  $x$ ,  $y$ , and  $z$  axes to represent all the three-dimensional rotational space. Then the orientation averaged

interaction potential is evaluated using Boltzmann weighting. Using these different weights, the orientation averaged interaction potential is evaluated, and this potential is used to compute the collision cross section.

For the calculations of collision cross section of ions, it is assumed that the DFT optimized structures are rigid. To ensure that the assumption is valid for the ammonium cations investigated in the present study, the collision cross sections of two extreme conformations for the largest two ionic molecules, acetylcholine and (3-carboxypropyl)trimethylammonium, are estimated. The DFT calculated electronic energies reveal that the extended structures of both acetylcholine and (3-carboxypropyl)trimethylammonium are unstable by 4.24 and 0.547 kcal/mol, respectively, compared to cyclic structures shown in Figure 2. The maximum difference between two conformations of (3-carboxypropyl)trimethylammonium is calculated as  $\sim 7$  Å<sup>2</sup>, which we can set as a maximum error bound originating from the structural uncertainty.

## RESULTS

**Mass-Mobility Correlation of Ammonium Cations.** IMS spectra were obtained as described above. The drift times of the ammonium cations were determined from the location of the peak maximums. Figure 1 shows example spectra taken with pure solvent being introduced to the electrospray needle and with 300  $\mu$ M *N,N*-dimethylammoniummethanol dissolved in the solvent. These spectra are characteristic of those considered in this work. Measured drift times, reduced ion mobilities (in N<sub>2</sub> drift gas), and determined  $\Omega_D$  for the nine ammonium cations chosen for this study are listed in Table 1 along with their respective molecular weights. The 12-4 potential model, which has proven satisfactory to model experimental data<sup>14,15,20-22</sup> has been used for the analysis of the experimentally determined mobilities of ammonium cations. The potential is expressed as

$$\Phi(r) = \frac{\epsilon}{2} \left\{ \left( \frac{\sigma - a}{r - a} \right)^{12} - 3 \left( \frac{\sigma - a}{r - a} \right)^4 \right\} \quad (6)$$

where  $\epsilon$ ,  $r$ , and  $\sigma$  are defined above and the parameter  $a$  is the location of center charge from the center of mass in the ion. Rearrangement of eq 6, along with the substitution of the appropriate constants, yields

$$K_0^{-1} = (1.697 \times 10^{-4}) (\mu T)^{1/2} \sigma^2 \Omega^{(1,1)*} \quad (7)$$

which gives the reduced ion mobility in terms units of cm<sup>2</sup> V<sup>-1</sup> s<sup>-1</sup>.  $\Omega^{(1,1)*}$  is the dimensionless collision integral, where  $\Omega_D = \pi \sigma^2 \Omega^{(1,1)*}$ . Derivation of eq 7 from eq 6 is well described by Johnson et al.<sup>14</sup> Equation 7 was fit to the data set of ammonium ion mobilities in N<sub>2</sub> using a nonlinear least-squares fitting procedure.<sup>14</sup> The plot of  $K_0^{-1}$  versus ion mass for ammonium cations drifting in N<sub>2</sub> is shown in Figure 2 along with the best fit to the data. As seen in Figure 2, all nine ammonium cations investigated in the present study exhibit a good correlation ( $R^2 = 0.99$ ) between mass and mobility of ion. In particular, the two different classes of ammonium cations (tertiary and quaternary) investigated in this study exhibit a common mass mobility correlation. Further, the

(31) Becke, A. D. *J. Chem. Phys.* **1993**, *98*, 5648–5652.

(32) Lee, C. T.; Yang, W. T.; Parr, R. G. *Phys. Rev. B* **1988**, *37*, 785–789.

(33) Harihar, P. C.; Pople, J. A. *Chem. Phys. Lett.* **1972**, *16*, 217–219.

(34) Olney, T. N.; Cann, N. M.; Cooper, G.; Brion, C. E. *Chem. Phys.* **1997**, *223*, 59–98.

(35) Rappe, A. K.; Casewit, C. J.; Colwell, K. S.; Goddard, W. A.; Skiff, W. M. *J. Am. Chem. Soc.* **1992**, *114*, 10024–10035.

(36) Graham, C.; Imrie, D. A.; Raab, R. E. *Mol. Phys.* **1998**, *93*, 49–56.

(37) Dugan, J. V.; Palmer, R. W. *Chem. Phys. Lett.* **1972**, *13*, 144–149.

(38) Dugan, J. V.; Magee, J. L. *J. Chem. Phys.* **1967**, *47*, 3103–3112.

(39) Bowers, M. T. *Gas Phase Ion Chemistry*; Academic Press: New York, 1979; Vol. 1.

**Table 1. Drift Times, Reduced Mobilities, and Collision Cross Sections of Ammonium Cations in N<sub>2</sub> Drift Gas**

ammonium cation	MW <sup>a</sup>	DT <sup>b</sup>	K <sub>0</sub> <sup>c</sup>	Ω <sub>D</sub> <sup>d</sup>
trimethylammonium	60	12.1	2.15	91.2
tetramethylammonium	74	12.7	2.04	95.3
trimethylethylammonium	88	13.4	1.93	102.2
<i>N,N</i> -dimethylammoniummethanol	90	13.4	1.93	100.9
choline	104	14.1	1.84	104.5
<i>N,N</i> -dimethylglycine	104	14.1	1.84	102.3
betaine	118	14.7	1.76	105.3
acetylcholine	146	16.3	1.59	118.5
(3-carboxypropyl)trimethylammonium	146	16.4	1.58	115.9

<sup>a</sup> Molecular weight (amu). <sup>b</sup> Drift time (ms). <sup>c</sup> Reduced mobility (cm<sup>2</sup> V<sup>-1</sup> s<sup>-1</sup>). <sup>d</sup> Collision cross section (Å<sup>2</sup>).

heteroatomic complements of the molecular ions do not impact the mass–mobility correlation.

**Tertiary and Quaternary Ammonium Cations with Similar Molecular Weights.** Two sets of cations, which have similar molecular weights but different structures, were chosen to investigate the influence of the composition and structural details of the ion on the mobility. The molecular weights of trimethylethylammonium and *N,N*-dimethylammoniummethanol are 88 and 90 amu, respectively. There is a significant structural difference between these two ions in addition to variation in the degree of alkylation to the ammonium groups. Protonated *N,N*-dimethylammoniummethanol possesses a hydroxyl group at the ethyl group while trimethylethylammonium possesses only alkyl groups. The molecular weights of choline and *N,N*-dimethylglycine cation are both 104 amu. Protonated *N,N*-dimethylglycine cations contain a carboxyl group while choline possesses a hydroxyl group. Experimentally determined mobility values of trimethylethylammonium and *N,N*-dimethylammoniummethanol are identical at 1.93 cm<sup>2</sup> V<sup>-1</sup> s<sup>-1</sup>. Mobilities of both choline and *N,N*-dimethylglycine cation are measured as 1.84 cm<sup>2</sup> V<sup>-1</sup> s<sup>-1</sup>. It is inferred that the contribution of the oxygen atom to the mobility (ion–neutral ion–neutral interaction) is not significantly different from that of a methylene group in the investigated ammonium cations.

**Functional Group Isomers of Ammonium Cations.** Two functional group isomers, acetylcholine and (3-carboxypropyl)-trimethylammonium cation, were examined to study the influence of the location of oxygen atoms on the molecular ion's mobility. As seen in Figure 2, acetylcholine and (3-carboxypropyl)trimethylammonium are not distinguishable based on their mobilities.

**Collision Cross Sections of Ions in N<sub>2</sub> via the Trajectory Method.** Theoretical Ω<sub>D</sub> of the ammonium cations investigated in this study were evaluated using the modified TJ method. Prior to application of the modified TJ method to the ammonium cations, we tested the model on previously published experimental data. Figure 3a shows the plot of experimentally determined Ω<sub>D</sub> of carboxylic acid anions<sup>15</sup> and abiotic amino acid cations<sup>14</sup> in N<sub>2</sub> versus those determined theoretically using the modified TJ method following the procedure described in the Experimental Section. Theoretical Ω<sub>D</sub> of both carboxylic acid anions and abiotic amino acid cations exhibit good agreement with experimental values. The agreement is within 5% in the worst-case deviation with less than 2% deviation on average. Figure 3b shows the plot of Ω<sub>D</sub> of ammonium cations obtained experimentally versus

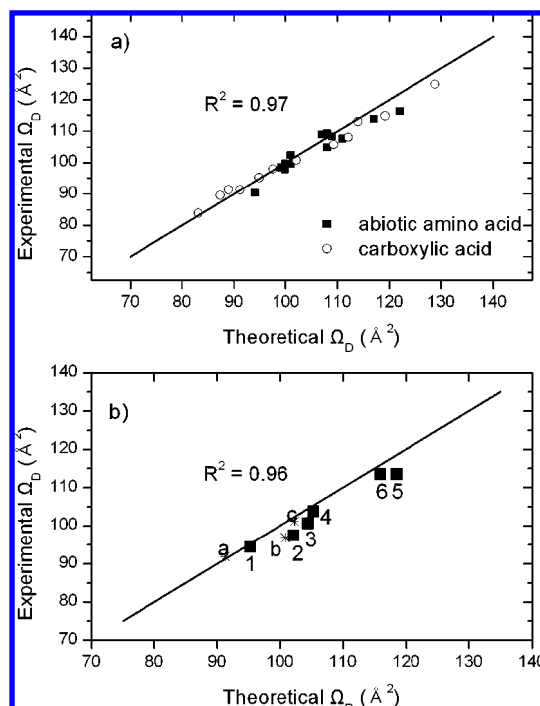


**Figure 3.** (a) Plot of experimentally determined collision cross sections (Ω<sub>D</sub>) of abiotic amino acid cations<sup>14</sup> and carboxylic acid anions<sup>15</sup> in N<sub>2</sub> versus theoretically determined Ω<sub>D</sub> using the modified TJ method for N<sub>2</sub> drift gas. Abiotic amino acid cation data are shown as solid squares and carboxylic acid anion data are shown as empty circles. The solid line is  $y = x$ . (b) Plot of experimentally determined collision cross sections (Ω<sub>D</sub>) of 3° and 4° ammonium cations in N<sub>2</sub> versus theoretically determined Ω<sub>D</sub> using the modified TJ method for N<sub>2</sub> drift gas. 3° ammonium cation data are shown as asterisks and 4° ammonium cation data are shown as solid squares. Each ion is labeled with the appropriate identifying number and alphabet shown in Figure 1. The solid line is  $y = x$ .

theoretical collision cross sections calculated using the modified TJ method. The worst observed deviation of the model from the experimental cross sections is 5% with an average deviation of 2.5%.

## DISCUSSION

**Classical Ion–Neutral Collision Model.** The cross section includes the information regarding the ion–neutral interaction. An ion and a neutral interact through the long-range ion induced dipole potential, which is given by

$$\Phi_{\text{IND}} = -\frac{(ze)^2\alpha}{2r^4} \quad (8)$$

where  $z$ ,  $\alpha$ , and  $r$  are defined above. The effective potential,  $\Phi_{\text{eff}}(r)$ , is expressed as  $\Phi_{\text{IND}} + L^2/2\mu r^2$ , where  $L$  is angular momentum of the collision partners about the center of mass of the combined system. The critical impact parameter  $b^* = (2\alpha e^2/\text{KE})^{1/4}$  is derived by setting KE equal to the maximum effective potential,  $\Phi_{\text{eff}}^*(r)$ , which is given by  $1/2(\text{KE})^2 b^4/\alpha e^2$ , where KE is the relative kinetic energy. Then the Langevin capture cross section is

$$\Omega_L = \pi(b^*)^2 = \pi\sqrt{\frac{2\alpha e^2}{KE}} \quad (9)$$

When the hard-sphere collision radius,  $R_c$ , is greater than  $b^*$ , the Langevin model is no longer appropriate and collisions are dominated by large angle deflections appropriate for a hard-sphere model. In this case, momentum transfer is no longer dominated by long-range interactions. In order to assess the ion–neutral collision under our experimental conditions,  $b^*$  and  $\Omega_L$  are evaluated from the mean relative kinetic energies. The evaluated  $\Omega_L$  and  $b^*$  are then compared to the experimental  $\Omega_D$  and  $R_c$  (Table 2). The hard-sphere collision radius  $R_c$  is determined from the experimental  $\Omega_D$  by equating it to  $\pi R_c^2$ . Experimental mean relative kinetic energies can be determined from the Wannier energy formula,

$$KE = \frac{1}{2}\mu g^2 = \frac{3}{2}k_B T + \frac{1}{2}Mv_d^2 \quad (10)$$

where  $M$  is mass of drift gas molecule and  $v_d$  is drift velocity of ion.<sup>40</sup> Under the current experimental conditions described in the Experimental Section,  $b^*$  is calculated on the order of 5 Å. Comparison with  $R_c$  shows that  $b^*$  in our system is on the same order, i.e., less than 1 Å smaller (Table 2). It is therefore inferred that the group of molecules studied here are on the borderline between being dominated by long-range versus short-range interactions, favoring some orbiting at lower collision energies, which would then determine the cross section for momentum transfer and hence the mobility.

**Computational Trajectory Method.** Ammonium cations investigated in this study exhibit a correlation between mass and mobility (Figure 2). In order to understand and estimate the effect of the each component of the ion–neutral interaction potential in terms of the observed mass–mobility correlation in our experimental system, theoretical calculations were performed using the modified TJ method. The collision cross sections ( $\Omega_D$ ) were evaluated using molecular ions with restricted interaction potentials and artificial charge distributions. Comparisons of the  $\Omega_D$  of tertiary (3°) and quaternary (4°) ammonium cations, abiotic amino acid cations, and carboxylic acid anions, which are calculated with different interaction potentials, are shown in Figures 4 and 5.

**Ion–Quadrupole Potential.** In order to understand the role of the ion–quadrupole interaction in ion–neutral interactions, the  $\Omega_D$  are computed without ion–quadrupole interactions. The presence of the quadrupole moment elevates the  $\Omega_D$  by 2.8% for the ammonium cations, 2.7% for the abiotic amino acid cations, and 4.2% for carboxylic acid anions (Figure 4a). Overall, it is observed that the addition of the ion–quadrupole potential to the model for ion–N<sub>2</sub> interaction improves the agreement between experimental and theoretical  $\Omega_D$  values. Previously, Su and Bowers reported quadrupole effects for molecules with high quadrupole moments using the average quadrupole orientation theory.<sup>41</sup> They demonstrated the significance of quadrupole effects, especially in the case when the ionic charge and quadrupole moment have

**Table 2. Critical Impact Parameter,  $b^*$ , Langevin Capture Cross Section,  $\Omega_L$ , and Mean Relative Kinetic Energies, KE, during the Experiments with Experimentally Determined Hard-Sphere Collision Radius,  $R_c$  for Each Ammonium Cation**

ammonium cation	KE (kcal/mol)	$b^*$ (Å)	$\Omega_L$ (Å <sup>2</sup> )	$R_c$ (Å)
trimethylammonium	1.70	5.08	81.0	5.41
tetramethylammonium	1.69	5.09	81.3	5.48
trimethylethylammonium	1.67	5.10	81.7	5.57
<i>N,N</i> -dimethylammoniummethanol	1.67	5.10	81.7	5.55
choline	1.65	5.11	82.1	5.66
<i>N,N</i> -dimethylglycine	1.65	5.11	82.1	5.67
betaine	1.64	5.12	82.5	5.75
acetylcholine	1.60	5.15	83.4	6.01
(3-carboxypropyl)trimethylammonium	1.60	5.15	83.5	6.01

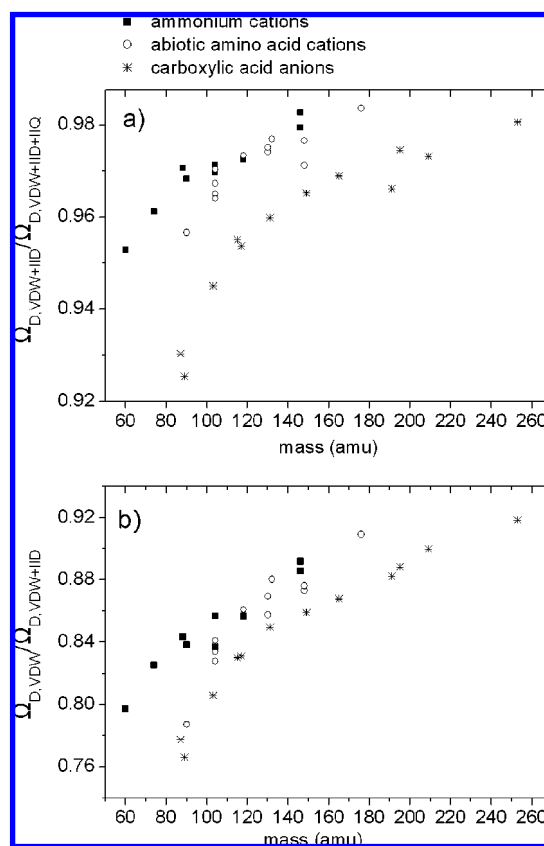


**Figure 4.** Plots of theoretically determined collision cross sections ( $\Omega_D$ ) (a) with potential from van der Waals and ion–induced dipole (VDW+IID) interactions over the theoretical  $\Omega_D$  with original pairwise potential, van der Waals + ion–induced dipole + ion–quadrupole (VDW+IID+IQ) interactions, and (b) with potential from van der Waals potential (VDW) over the theoretical  $\Omega_D$  with potential from van der Waals and ion–induced dipole (VDW+IID) interactions of 3° and 4° ammonium cations, abiotic amino acid cations, and carboxylic acid anions in N<sub>2</sub> versus ion mass. The ammonium cation data, the abiotic amino acid cation, and carboxylic acid anion data are shown as solid squares, empty circles, and asterisks, respectively.

the same polarity.<sup>41</sup> In analogy, a larger quadrupole effect is observed in carboxylic acid anions versus ammonium and abiotic amino acid cations, since nitrogen has a negative quadrupole moment. During the collision process, therefore, the change of a favorable orientation induced by the total ionic charge influences the collision cross sections via ion–quadrupole interaction. This

(40) Wannier, G. H. *Bell Syst. Tech. J.* **1953**, 32, 170–254.

(41) Su, T.; Bowers, M. T. *Int. J. Mass Spectrom. Ion Processes* **1975**, 17, 309–319.

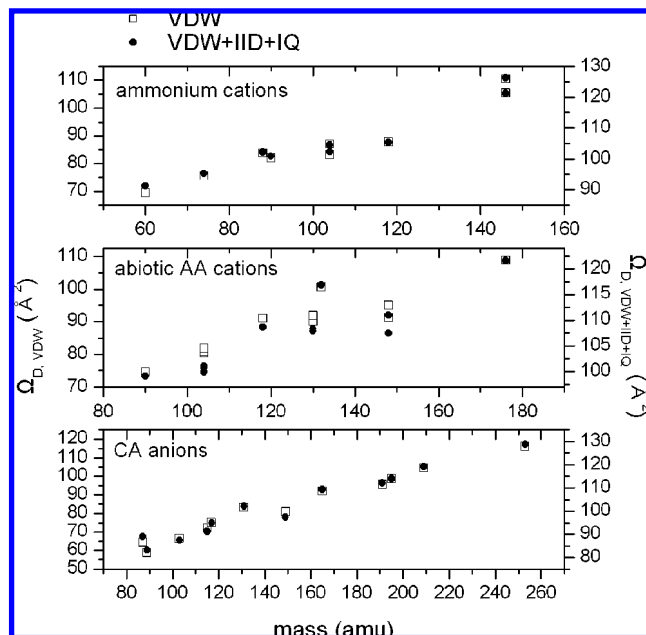


**Figure 5.** Plots of theoretically determined collision cross sections ( $\Omega_D$ ) of 3° and 4° ammonium cations, abiotic amino acid cations, and carboxylic acid anions in  $N_2$  versus ion mass. The calculated  $\Omega_D$  of the molecular ions only with van der Waals (VDW) interaction with  $N_2$  are shown as empty squares (left y-axis). The calculated  $\Omega_D$  of the molecular ions with original pairwise potential, van der Waals + ion-induced dipole + ion-quadrupole (VDW+IID+IQ) interactions, with  $N_2$  are shown as solid circles (right y-axis).

causes the observed difference of the  $N_2$  drift gas in ion-neutral interactions compared to spherical drift gas (i.e., He).

**Ion-Induced Dipole Potential.** In order to understand the effect of the long-range ion-induced dipole interactions between ions and neutral  $N_2$  molecules, theoretical collision cross section with the van der Waals and ion-induced dipole potential ( $\Omega_{D,VDW+IID}$ ) of molecular ions are compared to collision cross sections computed after assigning the total charge of the ionic molecule as neutral ( $\Omega_{D,VDW}$ ). The calculated  $\Omega_{D,VDW}$  with the van der Waals-only potential are ~8–23% smaller than the calculated  $\Omega_{D,VDW+IID}$ . The observed difference is attributed mainly to the lack of long-range interactions. Figure 4b shows plots of theoretically determined  $\Omega_{D,VDW}$  over the theoretical  $\Omega_{D,VDW+IID}$  of 3° and 4° ammonium cations, abiotic amino acid cations, and carboxylic acid anions in  $N_2$  versus ion mass. The agreement between the  $\Omega_{D,VDW}$  of ions and the  $\Omega_{D,VDW+IID}$  increases from 75 to 92% along with the mass of the molecular ion increases (Figure 4b). This is easy to rationalize since the contribution of the van der Waals interaction increases as the size (i.e., number of atoms) of the molecular ion increases. As a result, it can be concluded that the contribution of long-range ion-induced dipole interaction is important for the  $\Omega_D$  of small size molecular ions, while the van der Waals interaction prominently affects to the  $\Omega_D$  in large size molecular ions in this study.

**Van der Waals Potential.** The plots of the  $\Omega_D$  of 3° and 4° ammonium cations, abiotic amino acid cations, and carboxylic acid anions determined only with the van der Waals potential versus ion mass are shown in Figure 5, providing the comparison with the corresponding  $\Omega_D$  from original pairwise potential, which is the combined potential of van der Waals, ion-induced dipole, and

**Table 3. Theoretically Determined Collision Cross Sections of 3° and 4° Ammonium Cations**

ammonium cations	$\Omega_D^a$ (VDW <sup>b</sup> + IID <sup>c</sup> +IQ <sup>d</sup> )	$\Omega_D^a$ (VDW <sup>b</sup> + IID <sup>c</sup> )	$\Omega_D^a$ (VDW <sup>b</sup> )	$\Omega_D^e$ (center charge <sup>e</sup> )
trimethylammonium	91.2	86.9	69.3	91.3
tetramethylammonium	95.3	91.6	75.6	95.1
trimethylethylammonium	102.2	99.2	83.7	101.0
<i>N,N</i> -dimethylammoniummethanol	100.9	97.7	81.9	100
choline	104.5	101.5	87.0	104
<i>N,N</i> -dimethylglycine	102.3	99.2	83.0	101.7
betaine	105.3	102.4	87.7	105.3
acetylcholine	126.3	123.7	110.3	120.2
(3-carboxypropyl)- trimethylammonium	121.1	119.0	105.4	117.8

<sup>a</sup> Collision cross section ( $\text{\AA}^2$ ). <sup>b</sup> Van der Waals potential. <sup>c</sup> Ion-induced dipole interaction. <sup>d</sup> Ion-quadrupole interaction. <sup>e</sup> Ionic charge at center of mass.

ion-quadrupole interactions. It is notable that the characteristic relative  $\Omega_{D,VDW}$  show high similarity to the relative  $\Omega_D$  from the original theoretical calculations. It is inferred that the distinction between the  $\Omega_D$  for each ion is largely due to the short-range van der Waals interaction between ion and neutral  $N_2$  molecule. The molecular weight and specific geometry of the ions is considered to dominate the short-range van der Waals interaction, which affect the collision cross section of the ion.

**Mass-Mobility Correlation.** It has been suggested from the classical ion-neutral collision calculation that our ion-neutral collision occurs at the borderline between systems dominated by either long-range or short-range interactions. This is well supported from the theoretical investigation using the TJ method. The contribution of long-range interaction to the  $\Omega_D$  of ammonium cations is large (~30%) for small ions and decreases to less than 10% as the size of the ion increases.

Previous studies have suggested that charge localization on certain functional groups and the specific structure of the ion play major roles in the interaction between ions and neutral gas molecules in IMS.<sup>7–9</sup> In order to assess the effect of specific charge distribution in the molecular ion on  $\Omega_D$ , the ionic  $\Omega_D$  were evaluated after assigning the charge of the molecular ion at the center of mass. In general,  $\Omega_D$  of ions, in which a total charge +1 has been assigned at the center of mass in the molecule exhibit insignificant deviations from the  $\Omega_D$  of the ions determined with DFT calculated Mulliken charge distributions. The  $\Omega_D$  of the ammonium cations with the charge at the center of mass show an average deviation of 0.7% from the  $\Omega_D$  of ions with Mulliken charge distributions (Table 3). The  $\Omega_D$  of the carboxylic acid anions and abiotic amino acid cations exhibit 0.64 and 2.7% deviations, respectively, between the two models. This implies that the influence of the ion charge distribution on  $\Omega_D$  is minimal. The distance of the center of charge from the center of mass was calculated to investigate the specific charge distribution of the molecular ion in the present study. The average distance between the centers of charge from the centers of mass in the molecular ions is 0.7 Å for ammonium cations, and 0.9 Å for abiotic amino acid cations and carboxylic acid anions. It is inferred that the sizes of the molecular ions investigated in this study are too small to expect localization of the charge to a specific site.

In the previous section, we discussed that all potential terms, ion quadrupole, ion induced dipole, and van der Waals potential,



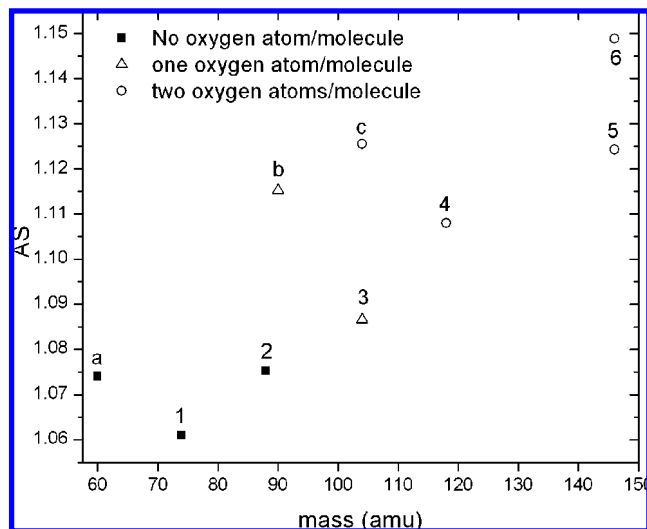


**Figure 6.** Plot of the total shape asymmetry (AS) of the ammonium cations versus ion mass. The ammonium cations with no oxygen atom are shown as solid squares. The ions containing one oxygen atom and two oxygen atoms are shown as empty triangles and empty circles, respectively. The DFT optimized structure of each numerically or alphabetically labeled ion is shown in Figure 2.

are important considerations in determining the collision cross section of the ions. Especially 75–95% of collision cross section is contributed by van der Waals interactions, which implies that strong mass–mobility correlations are highly affected by the geometries of the ions. This can explain the correlation observed in previous studies such as carboxylic acids and amino acids in terms of their structural similarity.<sup>14,15</sup> However, it is not able to explain the strong correlation among the ammonium cations. Localization of the charge in molecular ions induces specific gas-phase intramolecular cyclic structures of deprotonated carboxylate anions<sup>15,42</sup> and protonated abiotic amino acid cations.<sup>14</sup> However, DFT optimized structures of highly alkylated ammonium cations show no significant influence of the localization of the charge on the structures (Figure 2).

To evaluate the pure geometrical effect on the  $\Omega_D$ , we calculated the molecular volume and surface area of ions in  $N_2$ , which are also known as solvent-excluded volume and area,<sup>43</sup> using the Maximal Speed Molecular Surface (MSMS) program.<sup>44</sup> The volume and surface area of ion are traced by the inward-facing part of the probe sphere as it rolls over the ion.<sup>43</sup> The radius of the probe sphere is set to be the hard-sphere diameter of  $N_2$  molecule, 1.85 Å. A distinct mass–volume correlation among the ammonium cations with different numbers of oxygen atoms is found. However, the surface area demonstrates a higher correlation with ion mass for the overall mass range. For example, the volume increases 7.6 and 5.6% from trimethylethylammonium (88 amu) to choline (104 amu) and betaine (118 amu) while the surface area increases 6.1 and 6.8%, respectively. Using the obtained molecular volume and surface area, the molecular ion's asymmetry of the total shape is determined (Figure 6). The asymmetry of the total shape (AS) is expressed as

$$AS = \left( \frac{S}{4\pi} \right) \left( \frac{3V}{4\pi} \right)^{-2/3} = \frac{1}{4.836} \left( \frac{S}{V^{2/3}} \right) \quad (11)$$

where  $S$  and  $V$  are molecular surface area and volume, respectively. When the molecular ion is symmetrical (i.e., spherical) AS becomes unity, with AS increasing from unity as the asymmetry in shape increases. As seen in Figure 6, higher asymmetry is observed as the number of oxygen atoms and the size of the ion increase. Although the larger content of oxygen atom makes for smaller molecular volumes, it increases the asymmetry of the total shape, which increases the surface area of the ion. It is therefore inferred that our observed strong mass–mobility correlation is largely due to geometrical factors. This allows us to comprehend the observed mass–mobility correlation among two different classes of ammonium cations with the heteroatom complements in the present study.

## CONCLUSIONS

A high correlation between mass and mobility in  $N_2$  is observed from a number of tertiary and quaternary ammonium cations. The classical ion–neutral collision calculation implies that the group of molecules studied here are on the borderline between being dominated by long-range versus short-range interactions, favoring some orbiting at lower collision energies, which would then determine the cross section. Theoretical investigation using a modified trajectory method (TJ method) also indicates that all potential terms, ion quadrupole, ion–induced dipole, and van der Waals potential, are important considerations in determining the collision cross section of the ions. For the smaller molecular ions, the importance of long-range interaction is emphasized, while short-range interactions dominate the collision cross sections of the larger molecular ions. The evaluated volume and surface area suggest that shape asymmetry of the ammonium cations plays a small but significant role in determining the observed correlation between mass and mobility. The increase of the asymmetry in the shape of an ion compensates the reduction of the ion's volume, which finally yields similar mobilities of the ammonium cations with similar molecular weight investigated in this study, independent of their heteroatom complement.

## ACKNOWLEDGMENT

This research was carried out at the Jet Propulsion Laboratory, California Institute of Technology, under a contract with the National Aeronautics and Space Administration (NASA), the Noyes Laboratory of Chemical Physics, California Institute of Technology, and the Material and Process Simulation Center, Beckman Institute, California Institute of Technology. Financial support through NASA's Astrobiology Science and Technology Instrument Development, Planetary Instrument Definition and Development, and Mars Instrument Development programs is gratefully acknowledged. We appreciate the support provided by the Mass Spectrometry Resource Center in the Beckman Institute. The authors greatly appreciate Prof. Martin Jarrold at Indiana University Bloomington for generously allowing us to use and modify the Mobcal program. Hyungjun Kim and Hugh I. Kim contributed equally to this work.

(42) Woo, H. K.; Wang, X. B.; Lau, K. C.; Wang, L. S. *J. Phys. Chem. A* **2006**, *110*, 7801–7805.

(43) Connolly, M. L. *J. Am. Chem. Soc.* **1985**, *107*, 1118–1124.

(44) Sanner, M. F.; Olson, A. J.; Spehner, J. C. *Biopolymers* **1996**, *38*, 305–320.



**NOTE ADDED AFTER ASAP PUBLICATION**

The paper was posted on the Web on February 16, 2008. Equation 1 was replaced. The paper was reposted on February 21, 2008.

Received for review September 7, 2007. Accepted January 9, 2008.

AC701888E